ARTICLE

Integrated Nanoplasmonic Sensing for Cellular Functional Immunoanalysis Using Human Blood

Bo-Ram Oh,[†] Nien-Tsu Huang,[†,‡] Weiqiang Chen,[†] Jung Hwan Seo,[†,§] Pengyu Chen,[†] Timothy T. Cornell,[⊥] Thomas P. Shanley,[⊥] Jianping Fu,[†,∥] and Katsuo Kurabayashi[†,#,*]

[†]Department of Mechanical Engineering, University of Michigan, Ann Arbor, Michigan 48109, United States, [‡]Department of Electrical Engineering, Graduate Institute of Biomedical Electronics and Bioinformatics, National Taiwan University, Taipei, Taiwan, [§]Department of Mechanical and Design Engineering, Hongik University, Seoul, South Korea, [⊥]Department of Pediatrics and Communicable Diseases, University of Michigan, Ann Arbor, Michigan 48109, United States, [∥]Department of Biomedical Engineering, University of Michigan, Ann Arbor, Michigan 48109, United States, and [#]Department of Electrical Engineering and Computer Science, University of Michigan, Ann Arbor, Michigan 48109, United States

ABSTRACT Localized surface plasmon resonance (LSPR) nanoplasmonic effects allow for label-free, real-time detection of biomolecule binding events on a nanostructured metallic surface with simple optics and sensing tunability. Despite numerous reports on LSPR bionanosensing in the past, no study thus far has applied the technique for a cytokine secretion assay using clinically relevant immune cells from human blood. Cytokine secretion assays, a technique to quantify intercellular-signaling proteins secreted by blood immune cells, allow determination of the functional response of the donor's immune cells, thus providing valuable information about the immune status of the donor. However, implementation of LSPR bionanosensing in cellular functional immunoanalysis based on a cytokine secretion assay poses major challenges primarily owing to its limited sensitivity and a lack of sufficient sample handling capability. In this paper, we have developed a label-free LSPR biosensing technique to detect cell-secreted tumor necrosis factor (TNF)-α cytokines in clinical blood samples. Our approach integrates LSPR bionanosensors in an optofluidic platform that permits trapping and stimulation of target immune cells in a microfluidic chamber with optical access for subsequent cytokine detection. The on-chip spatial confinement of the cells is the key to rapidly increasing a cytokine concentration high enough for detection by the LSPR setup, thereby allowing the assay time and sample volume to be significantly reduced. We have successfully applied this approach first to THP-1 cells and then later to CD45 cells isolated directly from human blood. Our LSPR optofluidics device allows for detection of TNF-α secreted from cells as few as 1000, which translates into a nearly 100 times decrease in sample volume than conventional cytokine secretion assay techniques require. We achieved cellular functional immunoanalysis with a minimal blood sample volume (3 μL) and a total assay time 3 times shorter than that of the conventional enzyme-linked immunosorbent assay (ELISA).

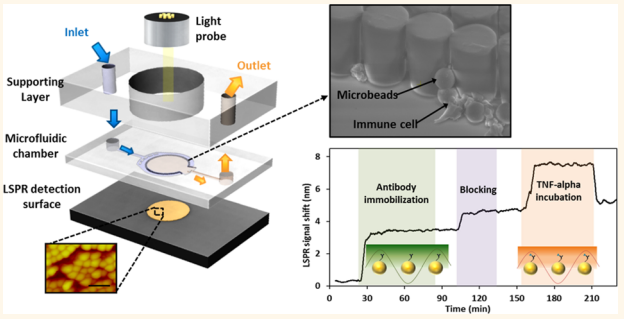

KEYWORDS: localized surface plasmon resonance (LSPR) · nanoplasmonic sensing · optofluidics · cellular immunoanalysis · tumor necrosis factor alpha (TNF-α)

Localized surface plasmon resonance (LSPR) is a plasmonic phenomenon that arises around nanoscale structures or nanoparticles of noble metals when light is illuminated onto a nanoscale-featured sensing surface. When the incident light frequency matches the natural frequency of electron oscillation of the conductive metal nanoparticles, the interactions between the incident light and the nanostructured surface modify the energy of the internal vibronic states of the particles and trigger the LSPR. Owing to the high sensitivity of the plasmon resonance to changes in the local refractive index, LSPR detection techniques have been implemented into various label-free quantitative analyses of antigen−antibody interactions, analyte surface density, and protein surface binding kinetics.[1−3] In LSPR, changes in the resonance wavelength and intensity signify the temporal or irreversible surface absorption of biological macromolecules, thus serving as biosensing signals.[4]

Cytokines, immunomodulating protein biomarkers secreted from immune cells, are

* Address correspondence to katsuo@umich.edu.

Received for review December 12, 2013 and accepted February 19, 2014.

Published online February 19, 2014
10.1021/nn406370u

indicators of the functional status of the human immune system. They play critical roles in regulating cell signaling, cell differentiation, and inflammatory response in the immune system.[5,6] For example, the cytokine secretion from immune cells in response to pathogenic invasions is an indicator of infection that shows a time-course change of the diseased condition of the human host.[7] However, such immune reactions are often extremely dynamic and occur quickly. Thus, a rapid immunoassay that affords comprehensive characterization and quantitative analysis of cytokines secreted from immune cells is the key to precisely determining the subtle variations and the dynamic characteristics of cellular immune functions in the host.[8,9]

The conventional enzyme-linked immunosorbent assay (ELISA) is a widely used method for quantification of cytokines. Benefiting from its cost-effective mass use, simple parallel array-type operation, and relatively high sensitivity, ELISA has become the most common tool for clinical diagnosis of pathogenic attacks on patients. However, the need for secondary antibodies binding to the target analytes results in a long sample preparation time and high complexity in sample labeling. Moreover, the fluorescent-based detection scheme requires a large amount of sample volume to achieve a sufficient signal-to-noise ratio for detection. Recent advances in the label-free surface plasmon resonance (SPR) detection technique overcame these shortcomings of ELISA by eliminating the tedious labeling process. However, the SPR detection technique still requires bulky instruments based on the Kretschmann arrangement, incorporating a prism coated with a thin metal layer and free space optics, while yielding a longer surface plasmon decay length (δ_d) than the LSPR technique. These features make the bedside application of the SPR technique challenging. The need for bulky optical components in the SPR technique hinders the detection platform from being miniaturized and integrated with other systems such as point-of-care microfluidic devices. While the longer surface plasmon decay length (δ_d) yields a higher sensitivity to a bulk refractive index change, it is less responsive to changes closer to the surface as compared to LSPR, which is essential for detecting antigen–antibody binding that occurs near the sensing surface.[10] The LSPR technique takes advantage of simple and cost-effective optics, which is highly desirable for microfluidic integration. More importantly, the LSPR technique yields precise and quick responses to the local refractive index changes resulting from the surface adsorption of target molecules. As such, it has been proven to be an effective *label-free* detection method for antibody–antigen binding.[11−14]

Both the detection limit and the sensitivity of the LSPR technique are highly dependent on the sensing platform and the size of the target molecule.[15,16] Cytokines are small molecules with a molecular weight of <30 kDa. The small size of cytokines greatly hinders the LSPR-based detection in clinical applications and disseminations. There have already been several approaches based on sandwich-type immunoassays with secondary antibodies or secondary particles to improve the detection limit of the LSPR technique for natural biomolecules.[13,17] However, these approaches lose the original advantage of label-free LSPR biosensing that enables rapid, dynamic biomolecular detection. To the best of our knowledge, quantitative analysis of immune cell-secreted cytokine molecules from human blood has never been demonstrated with an LSPR platform despite the advantage of the technique. The implementation of LSPR biosensing for human blood samples faces more challenges due to the presence of other complex blood components in addition to the immune cells and the analytes under study.

In this study, we developed an LSPR-based optofluidic immunoassay technique that could precisely determine the concentrations of small cytokine molecules secreted from immune cells in human blood with an ultrasmall sample volume and a much shortened assay time. Specifically, we successfully demonstrated an LSPR sensing platform device that could seamlessly allow isolating and trapping target immune cells from human lysed blood, cell incubation and stimulation, and detecting cell-secreted cytokines such as TNF-α on a single chip. Our technique employed an approach of spatially confining analytes within a small microfluidic chamber with a volume of a few microliters. This approach effectively increased the concentration of cytokines secreted from the trapped immune cells to a detectable range while compensating the limitations of the conventional LSPR technique for small-molecule detection. The enrichment of cytokines in such a small chamber volume further facilitated the analyte–antibody interactions and reduced the time required for achieving the equilibrium binding state.[18] As a result, the microfluidic LSPR immunoassay platform reported here achieved quantitative detection of cytokine secretion from a desired subset of immune cells down to a cell population as few as 1000 cells, which drastically reduced the sample volume by approximately 100 times and shortened the total assay time by 3 times as compared to the conventional cytokine secretion assays.

RESULTS AND DISCUSSION

LSPR Detection and Device Design. Again, LSPR arises when the frequency of the collective oscillation of electrons near the surface of a conductive metal nanoparticle matches the excitation light frequency. At the resonance wavelength, the light field induces a dipolar response of the conducting electrons as shown in Figure 1a. Binding of a biomolecule onto the surface of a noble metal (in this study, the metal is gold)

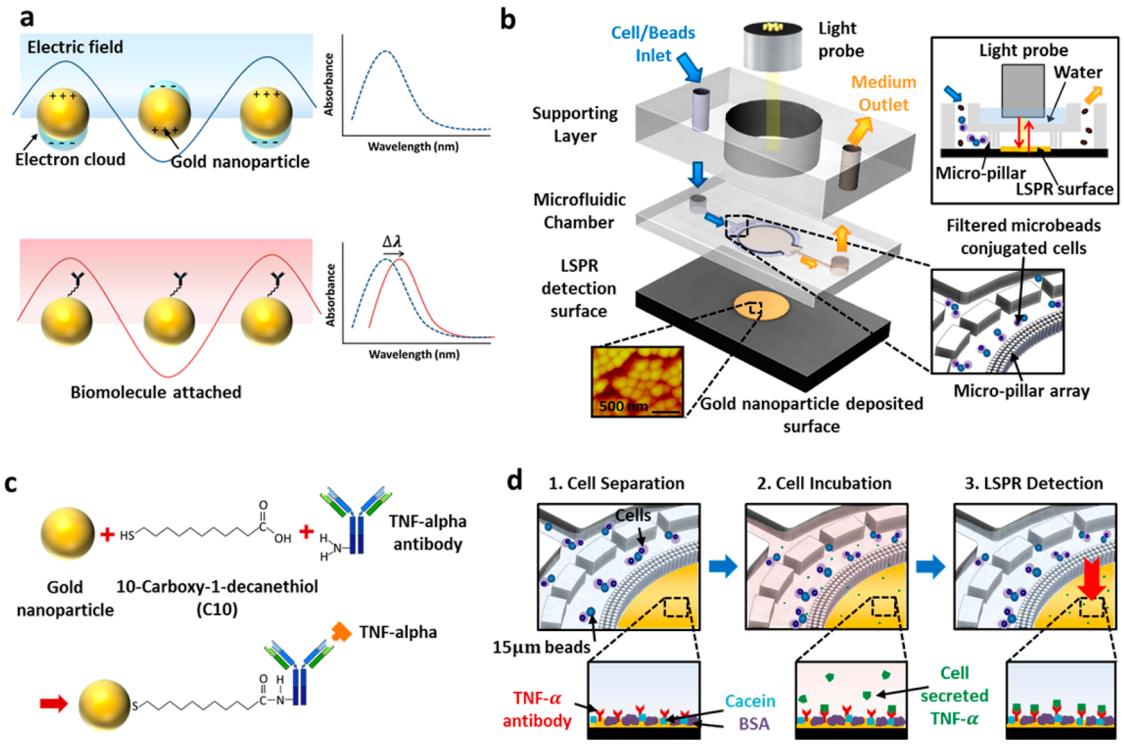

Figure 1. (a) Principle of nanoplasmoic biosensing based on LSPR at gold nanoparticle surfaces. (b) Schematic of the integrated LSPR optofluidic platform device. The bottom layer is a gold nanoparticle-deposited (or gold nanostructured) surface for LSPR detection. The magnified image (lower left) is an AFM image of the gold nanostructured LSPR detection surface. The gold nanoparticles are uniformly distributed on the sensor surface with a size distribution of 148.42 ± 17.98 nm and interparticular distance of 9.83 ± 2.93 nm. The middle layer includes a microfluidic chamber and channels. The chamber has integrated micropillar arrays (shown in the middle right schematic) to trap bead-bound target cells. The top layer provides structural support for light probe alignment and for cell/reagent injection and ejection. The cross-sectional schematic (upper right) shows the arrangement of the device and the light probe consisting of an illumination core and a bundle of detection optical fibers. (c) The gold nanostructured detection surface is functionalized with a chemical ligand (C10). The C10 ligand has a carboxylic group that binds with the amine group of the probe antibody molecule. (d) Concept of multifunctional LSPR optofluidic operation. Each illustration shows the soft lithographically patterned polydimethylsiloxane (PDMS) microstructures on the flipped side of the middle layer and the sensing surface of the bottom layer.

nanoparticle causes a change in the near-field refractive index around the nanoparticle. As a result, the absorbance of light changes, and this change results in a shift of the absorbance spectrum peak (Figure 1a). Such a LSPR spectrum wavelength peak shift is given by[19]

$$\Delta\lambda_{max} = m\Delta n\left[1 - \exp\left(\frac{-2d}{l_d}\right)\right]$$

Here m is the bulk refractive index response of the nanoparticles, Δn is the change in refractive index induced by the absorbate, d is the effective thickness of the adsorbed layer, and l_d is the characteristic electromagnetic field decay length.[19] The refractive index of the deposited monolayer of biomolecules is approximately 1.45,[20] which is higher than the refractive index of water medium. Thus, if there occurs a biomolecule binding event on the nanoparticle surface, Δn and d will increase, causing a red shift of the resonance peak wavelength.

Our optofluidic device was composed of two polydimethylsiloxane (PDMS) layers serving as a supporting layer and a microfluidic layer, respectively, and one LSPR sensing layer with a circular detection pattern of gold nanoparticles deposited at its center, which is shown as the yellow spot on the black bottom layer in Figure 1b and the AFM image. The gold nanoparticle detection surface was illuminated under a full spectrum of 400−700 nm light from the core of the light probe placed above the device. The reflected light from the sensing surface was collected by a bundle of optical detection fibers in the light probe (Figure1b, S1). The gold nanoparticles deposited on the sensing surface were functionalized with 10-carboxy-1-decanethiol (C10) and activated following the general 1-ethyl-3-(3-dimethylaminopropyl)carbodiimide (EDC) activation protocol.[21] The activated carboxylic group on the gold nanoparticles could then form esters with the amine groups on the primal antibody (Figure 1c).

The microfluidic chamber layer, mainly providing the function of trapping and incubating cells, is shown in the middle in Figure 1b. A unique circular structure composed of three arrays of micropillars with a pillar diameter of 30 μm and a pillar edge-to-edge gap distance of 5 μm was incorporated around the sensing

surface to isolate and enrich the target immune cells before the cells were stimulated and incubated for cytokine secretion and detection (Figure 1d, micropillar array). The diameter of the center region of the microfluidic chamber was set to be 3.2 mm, with a height of 50 μm. This chamber was connected to the inlet and outlet (0.75 mm in diameter) by channels of 200 μm and 50 μm in width and height, respectively. The total channel volume was calculated to be approximately 3 μL. Such a small chamber size enabled rapid accumulation and diffusion of cell-secreted cytokines and, therefore, acutely reducing the volume and incubation time required for the target analyte binding to the LSPR sensing surface. The top supporting PDMS layer provided structural support for injecting the sample with a syringe pump and sustaining a water cap filling the gap between the light probe and the detection surface (Figure 1b panel in the top right). The water cap served to minimize the refractive index mismatch at the interfaces, to increase the signal-to-noise ratio by suppressing background noise arising from thermal gradients and air fluctuations,[22] and to prevent direct contact between the probe and the sensing surface.

Figure 1d illustrates the processes of the label-free LSPR optofluidic cellular functional immunoanalysis technique developed for human blood samples. Our technique integrated cell isolation and enrichment, cell stimulation and incubation, and detection of cytokines secreted from isolated immune cells on a single chip. The general assay steps using the device are described as follows: The target cells were first attached to 15 μm diameter polystyrene beads conjugated with antibodies specifically binding to the cells' surface marker proteins. The bead-bound cells were then introduced into the device from the inlet, trapped by the micropillar arrays owing to the mechanical rigidity of the beads, and incubated in the microfluidic chamber. After stimulated by endotoxin solution for 2 h, the cells produced cytokines (*e.g.*, TNF-α), which readily diffused into the detection surface through the gaps between the micropillars and were captured by the primary antibodies covalently immobilized on the nanostructured gold surface (Figure 1d). Binding of the cytokines on the nanostructured gold surface altered the LSPR absorbance spectrum of the detection spot. We measured the spectrum peak shift using a custom-built LSPR detection setup shown in Figure S1. The illumination fiber in the light probe was connected to the broad-spectrum light source and used to excite the detection surface to induce the LSPR effect. The reflected light was then collected by the detection fibers also embedded in the light probe, and the light signal was collected by the spectrometer and converted to electrical signals for further analysis.

On-Chip Cell Trapping Performance. On-chip cell trapping with our LSPR device was demonstrated first for a human acute monocytic leukemia cell line (THP-1) and then for CD45+ immune cells isolated directly from lysed human blood as shown in Figure 2. THP-1 cells are commonly used as a model for mimicking the function and regulation of monocytes and macrophages and for immunocytochemical analysis of protein−protein interaction. CD45+ immune cells represent a group of immune cells that express CD45 surface marker, a type I transmembrane protein assisting in T-cell activation. The polystyrene microbeads were initially conjugated with antibodies that specifically interact with cell surface biomarkers: CD14 for THP-1 cells and CD45 for CD45+ immune cells in the lysed blood sample, respectively. The prepared microbeads were diluted to a concentration of 1.4×10^6 mL^{-1} in PBS and then mixed with THP-1 cells at a 1:1 ratio in the cell culture medium (RPMI) for 1 h to form immune cell−bead conjugated pairs. This process was repeated for CD45+ cells after a whole blood sample was red blood cell (RBC)-lysed, as shown in Figure 2a (also see Materials and Methods). The fluorescence microscopy image in the top panel of Figure 2b verifies that the immune cell−bead conjugation scheme worked in lysed blood. Here, the image shows that bead-bound CD45+ cells, freestanding immune cells, which could be either other immune cell subpopulations or unbound CD45+ cells, and residual RBCs were coexisting in the lysed blood sample.

We subsequently loaded the lysed blood sample into the device using a syringe infusion pump at a constant flow rate of 5 μL min^{-1}. The unbound cells and other components in the original blood escaped through the pillars and was washed out through the outlet (middle panel in Figure 2b, S2a) while the cells attached to the microbeads were efficiently captured by the micropillar arrays (the bottom panel in Figure 2b). The microbeads exhibited the capability of both isolating the target immune cells from the blood and ensuring high-fidelity cell trapping with the micropillar arrays. Mammalian cells are typically soft and elastic due to the lack of the rigid cellular wall possessed by plant cells. As a result, they can be easily deformed under external pressure and squeezed to escape through the gap between the micropillar arrays. In contrast, the microbeads behave as solid carriers and prevent the undesired escape of the target cells attached to them. As proved by the fluorescent intensity measurement of the cell population in the device (Figure 2c, S2b), the microbead attachment of cells enabled the trapping rate to reach nearly 95%, while unbound cells were trapped only at a rate of around 50% (Figure 2d). The image in Figure 2b shows that the cell-to-bead conjugation ratio is not necessarily 1:1 for all the pairs. However, this does not affect the accuracy of our method to quantify the trapping rate (see Materials and Methods).

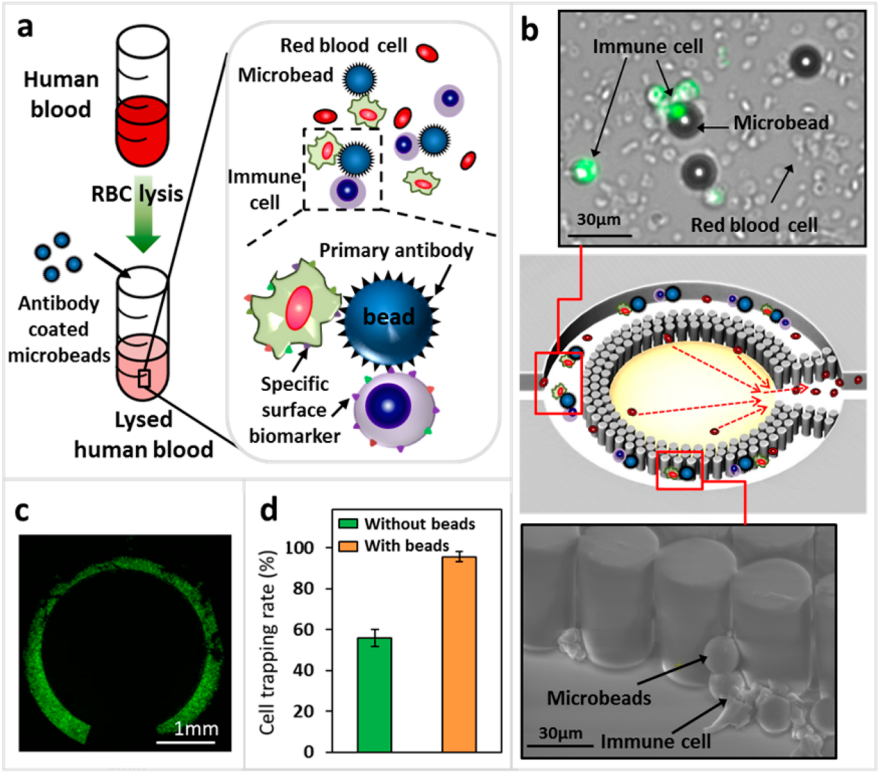

Figure 2. (a) Process of conjugating target immune cells with primary antibody-coated microbeads for their subsequent extraction from lysed human blood. Here, the human whole blood was first red blood cell (RBC)-lysed with the buffer to remove some fraction of the entire RBCs. The primary antibody-coated microbeads were then mixed with the lysed blood. Cells expressing a particular surface marker protein species were specifically bound to the microbeads. This process formed cell−bead conjugate pairs. (b) Process of isolating and trapping target white blood cells using micropillar arrays. The lysed blood sample containing the cell−bead conjugate pairs and residual RBCs was loaded into the device. The upper optical microscopy image shows bead-bound cells in the lysed blood sample. The lower scanning electron microscopy (SEM) image shows cell-carrying microbeads trapped by the micropillar arrays. (c) Fluorescence image showing the whole microfluidic chamber structure with trapped calceinAM-stained THP-1 cells. (d) Cell trapping rates for freestanding THP-1 cells and bead-bound cells. The cell−bead conjugation scheme increased the trapping rate up to 95% from 50% to 60%, which was achieved without the conjugation process.

We examined the viability of the cells trapped in the device using live/dead calceinAM stains under a fluorescent microscope before and after 4 h of incubation. The fluorescent intensity decreased only by 3.13 ± 0.21% after this incubation process. It follows that the cells incubated in the device were sufficiently healthy throughout the assay. Furthermore, our previous study[23] indicated that the microbead-bound cells secreted almost the same amount of cytokines during the on-chip incubation process. Thus, we can safely assume that the cytokine secretion performance of these cells virtually remains unaffected by the cell−bead conjugation process.

Dynamic Detection of Biomolecular Surface Binding. We selected purified natural TNF-α as the analyte cytokine species in our assay and characterized the device's performance for dynamic analysis of biomolecular surface binding events. The gold nanostructured detection surface of the device was first functionalized with anti-human TNF-α, which served as the capture antibody of the surface. The remaining uncovered detection surface was coated with blocking buffer containing 1% BSA and casein molecules to prevent nonspecific adsorption of TNF-α molecules. The TNF-α solution was then introduced to the device and incubated for 1 h to allow the analytes to fully engage with the primary antibodies. For each step described above, we thoroughly washed the LSPR detection surface with PBS solution to stabilize it against solvent annealing and avoid nonspecific binding of the introduced molecules to it. The LSPR peak wavelength throughout the entire process was continuously monitored (Figure 3). Exposure of the activated carboxy-terminal conjugated gold nanostructured surface to the anti-human TNF-α induced a red shift of 2.5−3.0 nm as a result of covalent ester group formation. Addition of the blocking buffer resulted in a weaker red shift (1 nm) mainly due to the smaller sizes of the BSA (MW ~66.5 kDa) and casein (MW ~28−32 kDa) than that of the antibody (MW ~150 kDa). Introducing 5.85 nM TNF-α yielded a further red shift because of the specific interactions between TNF-α and the antibody. The subsequent blue shift was possibly due to the removal of physically adsorbed TNF-α during rinsing. We further examined the selectivity of our sensing surface toward TNF-α by

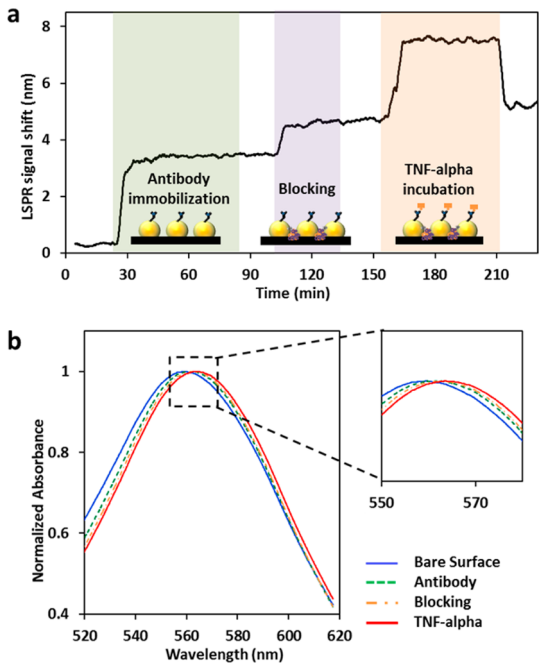

Figure 3. (a) Real-time LSPR signal shift during LSPR biosensor surface preparation and analyte detection processes. The green region shows the time-course absorbance spectrum peak shift of the LSPR detection surface during the primary antibody immobilization process with an incubation time of 60 min. The purple region shows the LSPR peak shift during the surface blocking process by BSA and casein molecules. The orange region shows the LSPR peak shift during the process of loading purified TNF-α to the detection surface with an incubation time of 60 min. At the end of each process, the entire detection surface was washed with PBS buffer to eliminate the nonspecific binding of reagent and analyte molecules. (b) Normalized LSPR absorbance spectra corresponding to the processes in (a).

introducing unpaired analyte, elafin, and a mixture of elafin and TNF-α analyte into the device (Figure3a, S3). The LSPR peak wavelength red-shifted only when TNF-α molecules were present in the solution (Figure 3a orange region, Figure S3a blue region), while no shift was observed with the other type of analyte, elafin, introduced (S3b purple region) to the detection surface. The total time required for the LSPR detection surface preparation prior to the assay was 2.5 h, which is much less than that of the conventional ELISA methods, which typically take an overnight process for detection surface preparation (Figure 3a).

TNF-α Standard Curve and Validation with ELISA. Prior to our LSPR cellular functional assays using real blood samples, we first obtained the analyte standard curve using a purified TNF-α (DY210, R&D Systems) solution of known concentration ranging from 100 to 500 ng/mL. With the increasing concentration of TNF-α, the LSPR peak wavelength shifted linearly from 0.1076 nm to 0.6779 nm (Figure 4a). This TNF-α standard curve provided the correlation between the analyte concentration and the LSPR spectrum peak shift. Additionally, we compared our LSPR immunoassay results with those obtained from the conventional ELISA method (DY210, R&D Systems) using a commercial plate reader (Synergy H1, BioTek) for four unknown concentrations of natural TNF-α samples (Figure S4). Each spectrum shift obtained from the LSPR detection was converted to a TNF-α concentration value using the standard curve in Figure 4a. Similarly, the conversion of the ELISA signal was performed using a calibration curve collected during the experiment. Figure S4 showed an excellent linear correlation (R^2 = 0.9528) between the results from the LSPR immunoassay and the ELISA analysis for the TNF-α samples.

Integrated Optofluidic LSPR Cellular Functional Analysis. After cross-validation of the biosensing performance of the LSPR platform with the ELISA technique, THP-1 cells suspended in buffer solution were loaded into the LSPR device for on-chip cell separation, incubation, stimulation, and detection of cell-secreted TNF-α. Figure 4b,c show results obtained from LSPR signal shifts due to binding of TNF-α secreted by LPS-stimulated cells with their population and the LPS concentration varied. The amount of TNF-α increased monotonically with the LPS concentration and the population of THP-1 cells incubated in the device. Incubation and stimulation of 20 000 THP-1 cells at an LPS concentration ranging from 5 to 25 ng/mL resulted in LSPR spectrum shifts of 0.1901, 0.3445, and 0.7004 nm, each corresponding to TNF-α secretion at a concentration of 163.36, 296.13, and 602.05 ng/mL, respectively. At an LPS concentration of 25 ng/mL, the LSPR signal shifted by 0.1761 nm (151.37 ng/mL), 0.3085 nm (265.14 ng/mL), 0.4412 nm (379.20 ng/mL), and 0.7235 nm (621.93 ng/mL) with 1000, 5000, 10 000, and 20 000 THP-1 cells, respectively (values inside the parentheses correspond to concentrations of TNF-α obtained from the standard curve). Under the same incubation and stimulation conditions, our optofluidic platform device allowed us to observe the TNF-α secretion from cells as few as 1000, which is 100 times less than that required in the conventional cellular immunophenotyping assay. The minimum cell population for detection, which is determined by measuring the LSPR spectrum shift equivalent to 3 times the standard deviation of the background noise from a blank device (without loaded cells), was about 533 cells. Typically, there exist on average 7000 leukocytes in 1 μL of human blood. It follows that our LSPR optofluidic platform yields a detection limit that permits the assay with a human blood volume as small as 100 pL.

A strong correlation (R^2 = 0.9793) was found between TNF-α secretion per cell and available LPS molecules per cell as shown in Figure 4d. A similar trend was also observed in our previous study that TNF-α secreted from each THP-1 cell was proportional to the number of LPS molecules available for each cell.[24] The number of LPS molecules available per cell decreases with the increasing cell population.

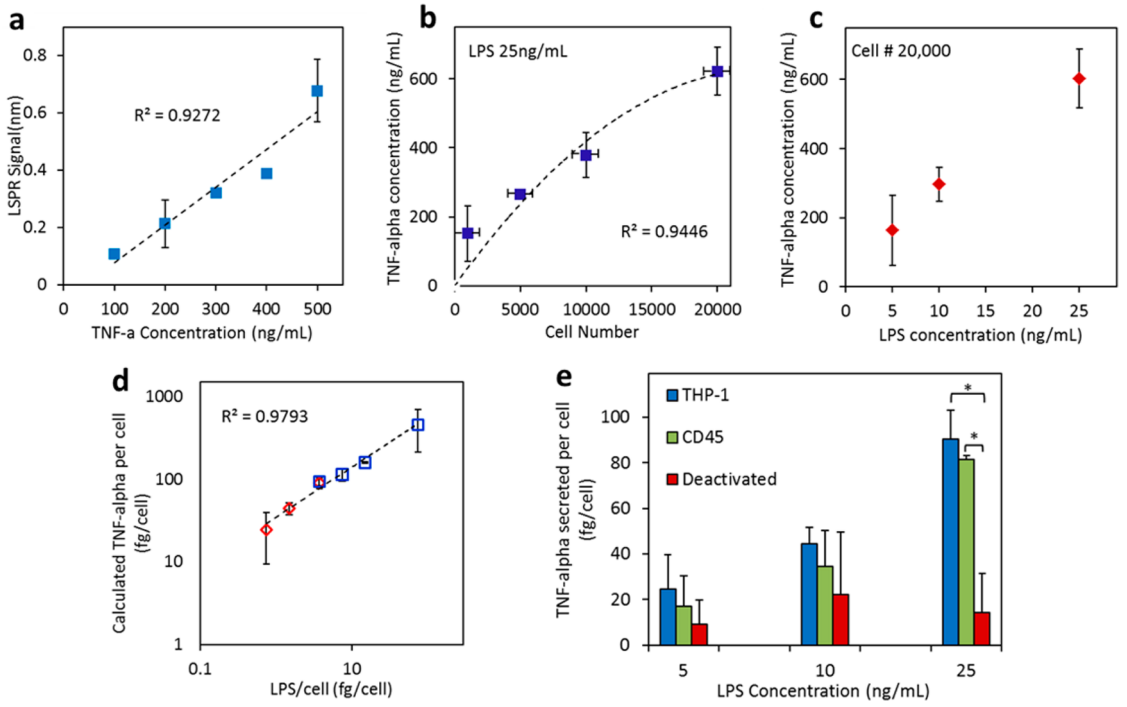

Figure 4. (a) Purified TNF-α standard curve. (b) TNF-α concentration *versus* population of trapped THP-1 cells upon LPS stimulation at 25 ng/mL. The minimum detectable cell population achieved by the LSPR optofluidic platform device is estimated to be 533 cells from curve extrapolation and background noise measurement. (c) TNF-α concentration *versus* LPS concentration upon stimulating THP-1 cells of a fixed population of 20 000. (d) Quantity of TNF-α molecules secreted per cell *versus* quantity of LPS molecules available for stimulation of each THP-1 cell. (e) Quantity of TNF-α molecules secreted per cell for normal THP-1 cells, CD45 cells, and LPS-deactivated cells loaded to and stimulated in the device at varying LPS concentrations. The *p*-values calculated using the paired Student's *t* test indicate significant differences ($p < 0.05$ (*)) in the TNF-α secretion behaviors of the functional and deactivated cells. All the plots were obtained from LSPR spectrum peak shifts of the detection surface of the optofluidic platform device.

This explains the saturation trend at the higher cell population in the curve of Figure 4b.

Now, it is possible that some TNF-α molecules secreted from the cells trapped near the channel outlet, as shown in Figure 2c, could escape from the LSPR sensor region of the device. To estimate an error resulting from this, we performed a control assay avoiding the on-chip cell isolation and trapping processes under the same conditions as our assay described above. In this assay, suspension, stimulation, and incubation of THP-1 cells were all performed outside the device using a 48-well plate. After the incubation process was completed, we collected only the supernatant of the cell suspension buffer from the plate, loaded it to our device, and performed the on-chip LSPR detection of TNF-α. By comparing the results between the control and original assays, we found that the discrepancy between the concentration of TNF- α secreted from the cells trapped and incubated in the device and the concentration of TNF-α collected from the supernatant was only 3%. Thus, the error was found to be negligible.

We further prepared cell cohorts consisting of normal THP-1, immunologically deactivated THP-1, and CD45+ cells isolated from human blood and measured the level of TNF-α secretion for these cohorts when stimulated at a given LPS concentration between 5 and 25 ng/mL. Previous research[25] reveals that immunologically "deactivated" peripheral blood monocytes may be functionally connected to immunoparalysis, which is associated with adverse outcomes of the severe reaction of a host to infection, such as sepsis. When a patient is in the state of immunoparalysis, the immune cells in the host body secrete an attenuated amount of cytokines. To examine whether our integrated LSPR platform could differentiate the normal and deactivated conditions, we deactivated THP-1 cells by treating them with 10 ng/mL of LPS in the RPMI medium overnight before LSPR biosensing assays. The cells were washed with cell growth media before being loaded into the device to remove the remaining LPS. This pretreatment of THP-1 cells with LPS increases the cells' endotoxin tolerance during the second LPS stimulation so that the cells become less sensitive to the stimulation.[26] As such, these deactivated THP-1 cells mimic the conditions resulting from the state of immunoparalysis. As shown in Figure 4e, after normal or deactivated THP-1 cells, both at a fixed population of 20 000, were introduced into the device and stimulated with varying LPS concentrations for 2 h, the number of TNF-α molecules secreted by the deactivated cells was 2−6 times

less than that from the normal THP-1 cells. Thus, our integrated LSPR optofluidic platform enabled quantitative differentiation of the two distinct THP-1 cell cohorts.

LSPR Optofluidic Human Blood Assay. CD45+ cells used in our immunofunctional assay were peripheral blood mononucleated cells (PBMCs) isolated from lysed human blood samples by using CD45 antibody-coated microbeads. These cells are a mixture of immune cells consisting of lymphocytes, monocytes, and macrophages. When exposed to LPS, not all of these cells respond to the stimulation. It follows that TNF-α secretion levels from THP-1 cells and CD45+ cells will be different under the same LPS stimulation with the same cell number. As can be seen from Figure 4e, the level of TNF-α secreted from THP-1 cells was 1.1−1.4 times higher than that from CD45 cells isolated from human blood samples. Moreover, TNF-α secretion levels from CD45+ cells obtained from a healthy donor were significantly higher than that from deactivated THP-1 cells mimicking the immunoparalysis state. Our results in Figure 4e demonstrate the promise of our LSPR optofluidic platform for future rapid monitoring and prognostic determination of infectious diseases based on on-chip human blood cellular immunofunctional analysis.

CONCLUSION

We have developed an optofluidic biosensing technique for cellular functional immunoanalysis based on nanoplasmonic LSPR detection. The multifunctional device used in our assay can achieve cell isolation and enrichment, incubation and stimulation, and detection of cell-secreted cytokines on a single chip platform. Our technique successfully demonstrated two noteworthy features. First, the developed technique enabled on-chip trapping of microbead-bound cells with at efficiency over 95% by its micropillar arrays. Using the develop LSPR platform device, we successfully demonstrated direct isolation of PBMCs from human blood samples and their immunofunctional analysis. Our technique allowed blood-sample assays by selectively trapping bead-bound CD45+ PBMCs inside a microfluidic chamber while filtering out other undesired blood components. Coupled with the microbead/micropillar-based cell trapping and isolation, our integrated LSPR optofluidic platform provided a means to achieve cellular functional immunoanalysis while eliminating laborious blood sample preparation. To the best of our knowledge, this study is the *first* to demonstrate human blood cellular immunophenotyping with the label-free LSPR nanoplasmonic detection technique. Second, our LSPR device is capable of leveraging the LSPR detection for rapid quantification of small-sized, physiologically relevant cytokines. Our on-chip assay technique incorporated the scheme of confining cells and analyte molecules within a small (3 μL) microfluidic chamber, which effectively maintained a high level of concentration even if the absolute number of TNF-α molecules presented to the detection surface was small. This spatial confinement scheme simultaneously achieved assay volume reduction and signal amplification to overcome the limited sensitivity of LSPR biosensing for cytokine detection. Additionally, the short diffusion path of analytes within the microfluidic chamber allowed the system to rapidly reach the equilibrium state.[18] This reduced the assay time for reagent incubation and LSPR sensing surface preparation, thus decreasing the total assay time. The whole assay process of our technique took only 4−5 h, whereas the conventional ELISA method could take nearly 2 days for the same cytokine secretion assay with immune cells.

The limited ability to detect the surface binding of small-sized analytes and the difficulty of handling the complex sample components have prohibited researchers from implementing the LSPR technique for cytokine secretion assays with human blood samples. Our study has successfully overcome these obstacles by the synergistic integration of microfluidic sample handling and separation and integrated LSPR biosensing. Our technique may open the door for a wider use of LSPR biosensing in clinical diagnosis of inflammatory diseases with a simple setup similar to the one used in this study. Co-detection of multiple cytokine species together with dynamic *in situ* monitoring of the cytokine secretion function of immune cells using an extended version of our technological platform could allow us to obtain new insight into cellular immunology in the future.

MATERIALS AND METHODS

Microfluidic Device Fabrication. The integrated optofluidic LSPR device consists of three different layers. The middle layer for cell separation and incubation chamber was fabricated using a micromachining technique by photolithography followed by a deep reactive ion-etching (deep silicon etcher, Surface Technology Systems, Allenton, PA, USA). The silicon mold was silanized with (tridecafluoro-1,1,2,2-tetrahydrooctyl)-1-trichlorosilane vapor (United Chemical Technologies) for 1 h under vacuum to facilitate subsequent release of PDMS structures from the mold. The PDMS prepolymer (Sylgard-184, Dow Corning) was prepared by thoroughly mixing the PDMS curing agent with the PDMS base monomer (wt:wt = 1:10), poured onto the silicon mold, and cured overnight in a 60 °C oven.[23] Fully cured PDMS structure was peeled off and treated with O_2 plasma for PDMS−PDMS bonding with the prepared supporting PDMS layer. The supporting PDMS layer is a 5 mm thick layer with no special features, except those for supporting fluidic interconnects for the device inlet/outlet and for sustaining the water cap between the light probe and the PDMS channel.

LSPR Sensor Chip Preparation. The LSPR signal detection sensor chip, Zeonor 8 spot array-SAM surface, was purchased from Lamdagen (Menlo Park, CA, USA). The LSPR sensor surface was activated with 20 μL of mixed 0.4 M EDC (1-ethyl-3-[3-dimethylaminopropyl]carbodiimide hydrochloride, Thermo Scientific) and 0.1 M NHS (*N*-hydroxysuccinimide, Thermo Scientific) at a 1:1 volume ratio in 0.1 M MES (1-ethyl-3-[3-dimethylaminopropyl]carbodiimide hydrochloride, Thermo Scientific) solution for 20 min. After the surface activation, the primary TNF-α antibody (DY210, R&D Systems) was diluted to 100 μg mL^{-1} in 1$\times$ PBS and 20 μL, injected to the detection surface, and incubated for 60 min. To eliminate the nonspecific binding on the detection surface, 20 μL of 1% BSA (albumin, from bovine serum, Sigma) in 1$\times$ PBS and 1$\times$ casein (5$\times$ casein block solution, Surmodics BioFX) blocking buffer were flown into the detection chamber and incubated for 20 min. During the entire process, the solutions were loaded using a syringe pump (LEGATO210, Kd Scientific)) at 5 μL min^{-1}, and between every step, the detection surface was thoroughly washed to remove any excessive solution or molecules using 40 μL of 1$\times$ PBS at 5 μL min^{-1}.

THP-1 Cell Culture, Reagents. THP-1 cells (TIB-202, ATCC) were cultured in RPMI (RPMI-1640, ATCC) growth medium supplemented with 0.05 mM 2-mercaptoethanol (21985-023, Life Technologies) and 10% fetal bovine serum (30-2020, ATCC). Cells were cultured at 37 °C with 5% CO_2 and 100% humidity, and the cell culture medium was replaced every 2−3 days. The cells were collected by centrifugation at a speed of 1200*g* and resuspended in RPMI for subsequent experiments.

Cell Quantification and Viability in the Device. The prepared THP-1 cells were stained by 1 μM calcein AM (C3100MP, Invitrogen) and incubated for 30 min before fluorescence microscopy imaging for cell quantification and viability test. A 130 W mercury lamp (Intensilight C-HGFIE, Nikon) was used for fluorescent illumination. Calcein AM was visualized with an FITC filter set (excitation 498 nm, emission 530 nm, Nikon). We employed two methods to quantify the cell population loaded in the device. First, we calculated the total number of cells introduced to the inlet by multiplying the original cell concentration with the total volume injected into the device. Hence, the population of isolated cells by the micropillars was estimated by subtracting the number of cells collected at the outlet. We also quantified the cell population by measuring the fluorescent intensity of the stained cells, which is proportional to the concentration of the fluorophore labeling the cells. We made control chambers, each with the same area and volume as the incubation chamber of the device, and loaded calcein AM-stained cells with their population varied. We obtained the standard curve showing the fluorescent intensity at each chamber as a function of the cell population. The fluorescent intensity integrated over the whole image of the cells in the chamber was then fit back to the standard curve to quantify the population of the cells loaded in the device.

Blood Sample Preparation and CD45+ Cell Captured with Polystyrene Microbeads. One milliliter of whole blood sample was incubated with 10 mL of RBC lysis buffer (00-4333-57, eBioscience) at a 1:10 volume ratio for 12−15 min. After the lysis, 20−30 mL of 1$\times$ PBS was added into the mixture and centrifuged at 400*g* for 10 min. We aspirated all the plasma and red blood cells and resuspended the remaining cells into RPMI medium. To prepare the polystyrene beads, 100 μL of biotinelated polystyrene beads (CP01N, Bangs Laboratory, Inc.) were washed with 1 mL of DI water three times and centrifuged at 1200*g* for 15 min in between. After the thorough washing, the beads were resuspended into 2 mL of washing buffer (0.1 M PBS (10$\times$ PBS), pH 7.4) and gently mixed with 80 μL of CD45 antibody (MHCD4515, Life Technologies) for 30 min at room temperature. After the incubation, the CD45 conjugated beads were washed three times as described above and made ready for use in capturing CD45 surface marker cells.

LSPR Detection Setup and the Spectrum Data Analysis. The LSPR sensor chip was illuminated by the light source (HL-2000 tungsten halogen light, Ocean Optics) that generates a continuous spectra of light from 400 to 700 nm. The incident light propagating along the illumination fiber embedded at the center of the light probe (R400-7-UV−vis, Ocean Optics) was introduced perpendicular to the sensing surface. The reflected light signal from the detection surface was collected by the detection fibers of the light probe, which was connected with a spectrometer (HR-4000, Ocean Optics) (Supporting 1). The absorbance spectrum of the detection surface was obtained using commercial signal processing software (Spectra Suits, Ocean Optics) that subtracts the measured intensity of the reflected light from the originally known intensity of the incident light at each wavelength over the spectral band of 400 to 700 nm. All the collected data were analyzed by a MATLAB code to obtain the regression curve and find the peak wavelength from the absorbance spectrum curve.

Conflict of Interest: The authors declare no competing financial interest.

Acknowledgment. J.F. and K.K. gratefully acknowledge financial support from the NSF Grant CBET 1263889 (J.F. and K.K.), CBET 0966723 (K.K.), and ECCS 1231826 (J.F.), and UMich-SJTU Collaboration on Biomedical Technologies (J.F. and K.K.). T.T.C. and T.P.S. gratefully acknowledge financial support from the NIH (K08HD062142). N.-T.H. gratefully acknowledges financial support by the National Taiwan University New Faculty Research Grant. J.H.S. acknowledges financial support from the 2014 Hongik University Research Fund. W.C. was partially supported by an American Heart Association Predoctoral Fellowship (13PRE16510018).

Supporting Information Available: Additional information as noted in the text. This material is available free of charge *via* the Internet at http://pubs.acs.org.

REFERENCES AND NOTES

1. Mayer, K. M.; Lee, S.; Liao, H.; Rostro, B. C.; Fuentes, A.; Scully, P. T.; Nehl, C. L.; Hafner, J. H. A Label-Free Immunoassay Based upon Localized Surface Plasmon Resonance of Gold Nanorods. *ACS Nano* **2008**, *2*, 687–692.
2. Bellapadrona, G.; Tesler, A. B.; Grunstein, D.; Hossain, L. H.; Kikkeri, R.; Seeberger, P. H.; Vaskevich, A.; Rubinstein, I. Optimization of Localized Surface Plasmon Resonance Transducers for Studying Carbohydrate-Protein Interactions. *Anal. Chem.* **2012**, *84*, 232–240.
3. Huang, T.; Nallathamby, P. D.; Xu, X. H. N. Photostable Single-Molecule Nanoparticle Optical Biosensors for Real-Time Sensing of Single Cytokine Molecules and Their Binding Reactions. *J. Am. Med. Assoc.* **2008**, *130*, 17095–17105.
4. Stuart, D. A.; Haes, A. J.; Yonzon, C. R.; Hicks, E. M.; Van Duyne, R. P. Biological Applications of Localised Surface Plasmonic Phenomenae. *IEE Proc.: Nanobiotechnol.* **2005**, *152*, 13–32.
5. Martins E Silva, J. Biochemical Characterization and Metabolic Effects of Tumor Necrosis Factor. *Acta Med. Port.* **1991**, *4*, 20–27.
6. Benton, H. P. Cytokines and Their Receptors. *Curr. Opin. iCell Biol.* **1991**, *3*, 171–175.
7. Boomer, J. S.; To, K.; Chang, K. C.; Takasu, O.; Osborne, D. F.; Walton, A. H.; Bricker, T. L.; Jarman, S. D. II; Kreisel, D.; Krupnick, A. S.; *et al.* Immunosuppression in Patients Who Die of Sepsis and Multiple Organ Failure. *J. Am. Med. Assoc.* **2011**, *306*, 2594–2605.
8. Chen, W.; Huang, N. T.; Li, X.; Yu, Z. T.; Kurabayashi, K.; Fu, J. Emerging Microfluidic Tools for Functional Cellular Immunophenotyping: A New Potential Paradigm for Immune Status Characterization. *Front. Oncol.* **2013**, *3*, 1–6.
9. Zhou, Q.; Kwa, T.; Liu, Y.; Revzin, A. Cytokine Biosensors: The Future of Infectious Disease Diagnosis? *Expert Rev. Anti-Infect. Ther.* **2012**, *10*, 1079–1081.
10. Shen, Y.; Zhou, J.; Liu, T.; Tao, Y.; Jiang, R.; Liu, M.; Xiao, G.; Zhu, J.; Zhou, Z. K.; Wang, X.; *et al.* Plasmonic Gold Mushroom Arrays with Refractive Index Sensing Figures of Merit Approaching the Theoretical Limit. *Nat. Commun.* **2013**, *4*, 2381.
11. Endo, T.; Yamamura, S.; Nagatani, N.; Morita, Y.; Takamura, Y.; Tamiya, E. Localized Surface Plasmon Resonance Based

Optical Biosensor Using Surface Modified Nanoparticle Layer for Label-Free Monitoring of Antigen–Antibody Reaction. *Sci. Technol. Adv. Mater.* **2005**, *6*, 491–500.
12. Endo, T.; Yamamura, S.; Kerman, K.; Tamiya, E. Label-Free Cell-Based Assay Using Localized Surface Plasmon Resonance Biosensor. *Anal. Chim. Acta* **2008**, *614*, 182–189.
13. Hall, W. P.; Ngatia, S. N.; Van Duyne, R. P. LSPR Biosensor Signal Enhancement Using Nanoparticle-Antibody Conjugates. *J. Phys. Chem. C* **2011**, *115*, 1410–1414.
14. Hiep, H. M.; Nakayama, T.; Saito, M.; Yamamura, S.; Takamura, Y.; Tamiya, E. A Microfluidic Chip Based on Localized Surface Plasmon Resonance for Real-Time Monitoring of Antigen–Antibody Reactions. *Jpn. J. Appl. Phys.* **2008**, *47*, 1337–1341.
15. Mayer, K. M.; Hafner, J. H. Localized Surface Plasmon Resonance Sensors. *Chem. Rev.* **2011**, *111*, 3828–3857.
16. Mitchell, J. Small Molecule Immunosensing Using Surface Plasmon Resonance. *Sensors* **2010**, *10*, 7323–7346.
17. Guo, L. H.; Kim, D. H. LSPR Biomolecular Assay with High Sensitivity Induced by Aptamer-Antigen-Antibody Sandwich Complex. *Biosens. Bioelectron.* **2012**, *31*, 567–570.
18. Salehi-Reyhani, A.; Sharma, S.; Burgin, E.; Barclay, M.; Cass, A.; Neil, M. A.; Ces, O.; Willison, K. R.; Klug, D. R. Scaling Advantages and Constraints in Miniaturized Capture Assays for Single Cell Protein Analysis. *Lab Chip* **2013**, *13*, 2066–2074.
19. Willets, K. A.; Van Duyne, R. P. Localized Surface Plasmon Reresonance Spectroscopy and Sensing. *Annu. Rev. Phys. Chem.* **2007**, *58*, 267–297.
20. Prime, K. L.; Whitesides, G. M. Self-Assembled Organic Monolayers: Model Systems for Studying Adsorption of Proteins at Surfaces. *Sci. Technol. Adv. Mater.* **1991**, *252*, 1164–1167.
21. Hermanson, G. T. *Bioconjugate Techniques*; Academic Press, 2008; pp 215–219.
22. Lazar, J.; Cip, O.; Cizek, M.; Hrabina, J.; Buchta, Z. Suppression of Air Refractive Index Variations in High-Resolution Interferometry. *Sensors* **2011**, *11*, 7644–7655.
23. Chen, W.; Huang, N.-T.; Oh, B.; Lam, R. H.; Fan, R.; Cornell, T. T.; Shanley, T. P.; Kurabayashi, K.; Fu, J. Surface-Micromachined Microfiltration Membranes for Efficient Isolation and Functional Immunophenotyping of Subpopulations of Immune Cells. *Adv. Healthcare Mater.* **2013**, *2*, 965–975.
24. Huang, N. T.; Chen, W.; Oh, B.-R.; Cornell, T. T.; Shanley, T. P.; Fu, J.; Kurabayashi, K. An Integrated Microfluidic Platform for *in Situ* Cellular Cytokine Secretion Immunophenotyping. *Lab Chip* **2012**, *12*, 4093–4101.
25. Cornell, T. T.; Sun, L.; Hall, M. W.; Gurney, J. G.; Ashbrook, M. J.; Ohye, R. G.; Shanley, T. P. Clinical Implications and Molecular Mechanisms of Immunoparalysis after Cardiopulmonary Bypass. *J. Thorac. Cardiovasc. Surg.* **2012**, *143*, 1160–1166.
26. Nimah, M.; Zhao, B.; Denenberg, A. G.; Bueno, O.; Molkentin, J.; Wong, H. R.; Shanley, T. P. Contribution of MKP-1 Regulation of p38 to Endotoxin Tolerance. *Shock* **2005**, *23*, 80–87.